

Soft x-ray driven femtosecond molecular dynamics

Etienne Gagnon¹, Predrag Ranitovic², Xiao-Min Tong³, C. L. Cocke², Margaret M.

Murnane¹, Henry C. Kapteyn¹, and Arvinder S. Sandhu^{1*}

¹*JILA, University of Colorado, Boulder, Colorado 80309-0441 USA*

²*J.R. Macdonald Lab, Physics Department, Kansas State University, Manhattan, KS 66506, USA*

³*Institute of Materials Science and Center for Computational Sciences, University of Tsukuba,*

Tsukuba, Ibaraki 305-8573, Japan

**E-mail: arvinder@jila.colorado.edu*

Abstract

The direct observation of molecular dynamics initiated by x-rays has been hindered to date by the lack of bright femtosecond sources of short-wavelength light. We used soft x-ray beams generated by high-harmonic upconversion of a femtosecond laser to photoionize a nitrogen molecule, creating highly excited molecular cations. A strong infrared pulse was then used to probe the ultrafast electronic and nuclear dynamics as the molecule exploded. We found that substantial fragmentation occurs through an electron-shakeup process, in which a second electron is simultaneously excited during the soft x-ray photoionization process. During fragmentation, the molecular potential seen by the electron changes rapidly from nearly spherically symmetric to a two-center molecular potential. Our approach can capture in real time and with angstrom resolution the influence of ionizing radiation on a range of molecular systems, probing dynamics that are inaccessible with the use of other techniques.

Ultrashort light pulses in the infrared (IR), visible, and near ultraviolet (UV) regions of the spectrum are used extensively in many experiments to uncover the detailed dynamics of the transition states involved in chemical reactions (1–5). To date, studies of this type have been limited to relatively low-lying electronic states in atoms and molecules that can either be directly excited by absorbing a visible/UV photon or indirectly excited with multiphoton excitation techniques (2–6). However, common processes in nature, such as photoionization of atmospheric molecules induced by soft x-ray solar irradiation, create highly excited states by selectively ejecting an inner-shell electron or by simultaneously exciting more than one electron in a molecule. These states are simply not directly accessible using visible or UV ultrafast photons. Indirect excitation with multiphoton techniques also cannot populate these highly excited states, because this approach tends to strip electrons in a stepwise manner, starting with the least-bound electrons. Therefore, to capture dynamics initiated by an ionizing event in an atom or molecule, a fast (femtosecond) pump pulse with a photon energy in excess of tens of electron volts is required. Such photoionization dynamics play an important role in the atmospheric chemistry of the planetary systems (7,8). Moreover, the physics of photoionization underlies virtually all interactions of ionizing radiation with matter.

This field of radiation chemistry, which seeks to understand how ionizing radiation interacts with chemical systems (9), has made considerable progress in the past decades through the use of synchrotron and plasma light sources. However, so far these studies have not achieved the femtosecond time resolution necessary to directly observe radiation-induced dynamics. Fourth-generation sources (e.g., ultrashort-pulse free-electron x-ray lasers) are currently being developed, in part to make such studies possible.

Laser-generated high-order harmonics can be used to produce bright, coherent beams of

shortwavelength light with ultrashort pulse duration. In high-harmonic generation, an intense ($>10^{14}$ W cm⁻²) femtosecond IR laser pulse is focused into a gas. The extreme nonlinear-optical interaction coherently upshifts the incident laser light into the soft x-ray and even the kiloelectron volt photon-energy range (10). Because photoabsorption cross sections for most molecules are largest for photon energies ranging from 12- to 120-eV (11), high harmonics are an ideal source for molecular excitation. Furthermore, their very short pulse duration and perfect synchronization with the driving laser pulse presents the intriguing possibility of studying electronic and nuclear dynamics with femtosecond and even attosecond resolution (12).

Up to this point, a few pioneering studies have used high-harmonic light to explore ultrafast dynamics in atoms (13), molecules (14,15), and solids (16). For example, in recent work a soft x-ray pulse was used to ionize and highly excite Xe, populating a number of shakeup states with low probability (13). The lifetimes of the resultant Auger decay were then confirmed to be 6 and 31 fs, in agreement with previous spectral measurements. In molecular systems, however, x-ray ionization can initiate complex dynamics that are much less well understood than in the atomic case, involving many excited and correlated electron channels that cannot be easily calculated and exhibiting complex spectra that cannot be understood on the basis of spectral measurements alone. Therefore, time-resolved measurements of x-ray driven dynamics in molecules can play a critical role in helping us to develop a better understanding of these concepts. However, ultrafast, femtosecond-duration x-rays have not previously been used as an ionizing pump beam to initiate dynamics in molecules. The available flux to date was simply too small to excite a sufficient fraction of molecules in any sample to use standard techniques, such as transient absorption spectroscopy, to observe x-ray-initiated dynamics.

Fortunately, other, more selective spectroscopic approaches can be successfully employed, as

we demonstrated using coincident electron-ion threedimensional momentum imaging. This technique efficiently collects ionized molecular fragments in coincidence, making it possible to fully reconstruct a single ionization and fragmentation event. This reaction microscope (17) technique has been used very successfully for a variety of studies of atomic and molecular processes, in both femtosecond-laser and synchrotron experiments (18, 19).

We used this type of reaction microscope (Fig. 1) to observe the dissociation of a molecule ionized by soft x-ray radiation in real time. In our experiment, a few-femtosecond soft x-ray pulse ionizes N₂ by ejecting an electron from the valence or inner valence shells. The molecule is left in one of the many highly excited states of N₂⁺, which then dissociate into an ion and a neutral atom. Using the reaction microscope, we can detect electrons and ions in coincidence, and from that information we can identify the different ionization and dissociation channels involved as the excited molecule explodes. We observed two main dissociation pathways; One pathway is reasonably well understood, and occurs when a soft x-ray ejects an inner valence ($2\sigma_g$ or $2\sigma_u$) electron from the N₂ molecule. The second dissociation pathway occurs when the soft x-ray removes an outer valence ($3\sigma_g$) electron, and a second electron is simultaneously excited in a process known as electron shakeup. These shakeup states in molecules have interesting features and fragmentation dynamics that have not been previously explored either theoretically or experimentally. We can follow the dynamics of these shakeup states as the molecule dissociates by using a short IR probe pulse to further ionize the excited N₂⁺ to the N₂²⁺ ground state, forming two N⁺ fragments. The reaction microscope then allows us to detect the kinetic energy of the

coincident N^+/N^+ ion pair as a function of time delay to follow the dissociation dynamics. Our soft x-ray pump–IR probe scheme thus makes it possible to map the electronic and nuclear dynamics of highly excited N_2^+ states with femtosecond time resolution and angstrom spatial resolution. By a comparison of these measurements with theoretical calculations, our results suggest that this fragmentation occurs predominantly via an antibonding shakeup state, where a loosely bound $4\sigma_u$ electron surrounds an exploding N_2^{2+} core. The loosely bound shakeup electron experiences a rapid transition from a nearly spherically symmetric initial molecular potential to a two-center potential and finally to a separate atom and ion at the dissociation limit. Furthermore, our data show evidence of three-body dynamics and quantum interferences resulting from the two-center nature of the molecular potential (20).

We generated high-harmonic light in a phase-matched geometry (21) by upshifting intense 2-mJ, 28-fs pulses centered at 800 nm from a 2-kHz ultrafast Ti:sapphire laser system (KMLabs, Boulder, CO) in a 2.5-cm-long, 150-mm-diameter hollow waveguide filled with Ar gas. The peak laser intensity in the waveguide was $\sim 10^{14} \text{ W cm}^{-2}$, and the argon pressure was typically 30 torr. A single harmonic order at a wavelength of 30 nm was selected from the comb of odd harmonics emerging from the waveguide and focused to $\sim 100 \mu\text{m}$ with two multilayer mirrors. This resulted in a pump beam of $\sim 43\text{-eV}$ photon energy with a few–electron volt bandwidth, a pulse duration of ~ 5 fs, and a flux of $\sim 10^6$ photons per pulse or 2×10^9 photons/s. Part of the laser output was split, delayed, and then recombined with the soft x-ray pump beam to serve as a colinear probe beam. The probe beam was focused using a 75-cm lens to a $\sim 100\text{-}\mu\text{m}$ -diameter spot with an intensity of $\sim 10^{12}$ to $10^{13} \text{ W cm}^{-2}$. The N_2 gas was cooled and confined using a supersonic jet expansion employing a $30\text{-}\mu\text{m}$ nozzle. The cold supersonic part of the jet was selected with a $300\text{-}\mu\text{m}$ skimmer placed ~ 8 mm from the gas nozzle. The gas density in the

interaction region was estimated to be 10^{11} molecules cm^{-3} . This experimental setup was run continuously with excellent stability and minimal loss in detector count rate for data-acquisition times of >100 hours.

The reaction microscope consists of an electrode configuration that generates a uniform electric field in the interaction region to accelerate reaction fragments toward the detectors. A magnetic field was also used to confine the fast moving electrons. The result was near-4p collection efficiency for both electrons and ions. The fragments were then detected by microchannel plates employing a position-sensitive delay-line anode (RoentDek, Kelkheim-Ruppertshain, Germany). These detectors record the position coordinates and time of flight of the fragments with spatial and temporal resolutions of ~ 100 μm and 500 ps, respectively. Together with the knowledge of the initial position of the reaction (defined by the interaction region) and the electric and magnetic fields, this information enables the reconstruction of all three components of momentum of each particle that hits a detector. Using this reaction-imaging apparatus, we accumulated electron and ion data for each laser shot. Post analysis of the data was then used to deduce electron-ion correlations and to implement coincidence conditions that filter the data to identify the different dissociation channels.

The photoionization of N_2 by x-rays can initiate a series of complex molecular dynamics. The ground state configuration of N_2 is $1\sigma_g^2 1\sigma_u^2 2\sigma_g^2 2\sigma_u^2 1\pi_g^4 3\sigma_g^2$ and our photon energy of 43 eV can remove both outer-valence ($3\sigma_g^2 1\pi_g^4$) and inner-valence ($2\sigma_g^2 2\sigma_u^2$) electrons. The inner-valence ionization pathway, schematically shown in blue in Fig. 2(a), results in the formation of many highly excited states of N_2^{+*} , with potential energies between typically 23 and 43 eV (relative to the N_2 ground state) (22). The cross sections for forming these states are known from synchrotron measurements (23). The finite bandwidth of our photon source does not allow us to

do resolve each state separately; however, previous work(22, 24-26) indicates that most of these inner-valence ionized molecules rapidly evolve to separated $N(2s^2,2p^3)$ and $N^+(2s^2,2p^2)$ fragments (i.e., electronic states with principal quantum number $n = 2$) (27). These dissociation channels are schematically represented by potential-energy curves that lie in the blue band shown in Fig. 2B.

Figure 2C plots ion- and electron-energy correlation map obtained for coincident fragments using the reaction microscope. We can identify the known dissociation pathways resulting from inner-valence ionization of the molecule using energy conservation: $E_{e^-} + 2E_{N^+} = h\omega_{x\text{-ray}} - E_{\text{limit}}$, in which the sum of the fragment kinetic energies [electron (E_{e^-}) and ion (E_{N^+}) + neutral] is equal to the soft x-ray photon energy ($h\omega_{x\text{-ray}}$) minus the energy corresponding to the dissociation limit (E_{limit}). Our data confirm that inner-valence hole states of the molecule decay to the $n = 2$ dissociation limit (events that lie between the blue lines in Fig. 2C) through channels that are indicated in Fig. 2B. The horizontal substructure at 14 eV of electron energy and 1 eV of ion energy is due to dissociation from inner-valence ionic states that lie in the range of 27 to 31 eV (28). This well-defined feature has also been observed in other studies as the F-band (25, 26).

Dissociation pathways that yield both a low-energy electron and a low-energy ion (indicated by events between the red lines in Fig. 2C) and that represent a very large fraction of dissociation events cannot be explained by the dissociation of inner-valence hole states. From energy-conservation arguments, these channels must represent a molecular excitation near the double-ionization threshold (~ 43 eV) that dissociates to a ground-state ion and an excited neutral atom, with the outer electron in an $n = 3$ principal quantum number state (red band in Fig. 2B). These pathways have not been investigated previously. We show below that these dissociation channels are consistent with fragmentation of excited states resulting from an electron-shakeup process

(Fig. 2A) accompanying outer-valence $3\sigma_g$ ionization.

To follow the time evolution of these shakeup states as they dissociate, as well as to uniquely identify them, we used a time-delayed IR probe pulse to eject a second electron from the molecule by multiphoton ionization. This second ionization step promotes the excited molecular ion (N_2^{+*}) to the doubly ionized (N_2^{2+}) ground state, which then explodes into two N^+ ions of equal and opposite momentum (29). The signature of this final product channel can be isolated from the data very effectively by detecting two N^+ ions in coincidence that have zero total momentum in the center-of-mass frame. Because we do not observe any counts in the correlated N^+/N^+ product channel in the absence of the IR field, we can cleanly probe the evolution of the N_2^{+*} dissociating wave packet, free of background contamination from other N^+ ions. By varying the pump-probe time delay, we interrupt the fragmentation of the N_2^{+*} at different times (i.e., different internuclear separations) (Fig. 3A). Using the reaction microscope to monitor N^+/N^+ coincidences, we can map the ion kinetic energy release (KER) as a function of time delay. The ion KER at any given time delay t between the soft x-ray pump and the IR probe is determined by the sum of the energy that the ions gain in the N_2^{+*} state (times $0 \rightarrow t$), as they evolve from the Frank-Condon region toward the dissociation limit, plus the energy gained after time t on the known N_2^{2+} dissociation curve (30). In a classical picture, we can thus write the ion KER as Eq.1

$$KER(t) = [E_1(r_0) - E_1(r_t)] + [E_2(r_t) - E_2(\infty)]; \quad (1)$$

where r_0 and r_t are the internuclear separations at time delay 0 and t respectively. Represents the potential-energy curve for N_2^{+*} ; and E_2 represents that for N_2^{2+} . The time-dependent KER data can then be used to deduce the characteristics and dynamics of the unknown excited state(s), namely the $E_1(r)$ curve (Fig. 3A).

We find that near zero time delay between the soft x-ray pump and IR probe, the N_2^{+*} wave

packet is instantly transferred to the N_2^{2+} potential-energy curve, leading to a large ion KER from 6 to 8 eV (Fig. 3B). The finite spread of KER data is a direct result of Frank-Condon vibrational spread of the wave packet released on the N_2^{+*} potential. The limiting values of KER are dependent on the exact shape of potential-energy surfaces in the Frank-Condon region, as explained later when we discuss our theoretical calculations. We observed that the ion KER decreases sharply as a function of time delay to ~ 4 eV within 150 fs. For large pump-probe time delays ≥ 300 fs, the ion KER does not change appreciably. This indicates that the excited N_2^{+*} has already evolved into two separate noninteracting fragments: a ground-state ion and an excited neutral atom. The low ion KER (~ 3 eV) at large time delays (internuclear separations) indicates that the states we are probing are highly excited states that, from energy conservation, must decay to the $n = 3$ limit (Fig. 2).

The observed time-resolved KER data can be explained by considering electron-shakeup processes, in which a second electron is simultaneously excited when a $3\sigma_g$ valence-shell electron is ejected by a soft x-ray (red in Fig. 2A). To support this hypothesis, we performed calculations to identify possible candidates for the highly excited N_2^+ states that formed as a result of a shakeup process. These states include Rydberg states (31) surrounding a doubly charged molecular core, as have been observed in near-threshold photoelectron spectra obtained by Krummacher *et al.* (22) in the energy range up to 40 eV. However, with the exception of binding energies, no further information has been reported on these states. Our calculations therefore construct these states to correspond approximately to a doubly ionized ground-state (N_2^{2+}) molecular core with an additional excited electron. For a given internuclear separation, we first calculated the effective potential of N_2^+ ions in the ground state by the multiple-scattering self-consistent method (32). The orbital energy of various excited shakeup states was calculated

using an effective potential with a Coulomb tail correction in the asymptotic region. Adding this orbital energy to the ground-state energy of N_2^{2+} (30), we obtained the potential-energy curves for the excited shakeup states. (Fig.4). These states are populated when the electron in a $3\sigma_g$ state is ejected by a 43-eV photon, and a second valence $3\sigma_g$ electron is promoted to the higher valence levels $3\sigma_u$, $4\sigma_u$, $4\sigma_g$, and assorted p orbitals. The electron state corresponding to a $4\sigma_u$ shakeup (black curve in Fig. 4) is closest to the N_2^{2+} ground state and has the largest overlap with the valence $3\sigma_g$ orbital. Hence, this state is most likely to be populated in the Frank-Condon region as a result of an electron shakeup process. This state then decays to the dissociation limit, with the final configuration of fragments corresponding to an ion $N^+(^3P)$ and a neutral N atom ($n = 3$).

Choosing this $4\sigma_u$ electron state (Fig. 4) as a likely candidate for $E_1(r)$ in Fig. 3A, we calculated the KER at different stages of fragmentation using Eq. 1 and the derivative in Eq. 2 (where μ is the reduced mass)

$$dr_t / dt = \text{sqrt}[2(E_1(r_0) - E_1(r_t)) / \mu] \quad (2)$$

The N^+/N^+ KER data obtained from theory is in the form of a band of finite width, and the two limits are overlaid as black lines on the experimental data in Fig. 3B. These KER limits correspond to two limiting values of the radius of the N_2^{+*} wave packet launched by soft x-ray excitation (Fig. 3A). The slope of the N_2^{+*} potential in the Frank-Condon region implies that excitation at smaller internuclear distances leads to higher KER. The upper limit of the KER is thus set by the width of the parent N_2 ground-state wave packet. The lower limit is imposed by the condition that the wave packet has to overcome the local potential minimum on the N_2^{+*} potential, as well as the potential barrier of N_2^{2+} for time delays near zero (Fig. 3A). These restrictions lead to the distinctive KER spectra shown in Fig. 3B. The excellent agreement

between theory and experiment in Fig. 3B demonstrates that the 4su orbital, because of its large overlap with the valence shell, is a major excitation and fragmentation channel for soft x-ray excited N₂ molecules. This dissociation channel and its dynamics have not been yet identified or explored.

Next, we interpreted the finer features of the shakeup-state dissociation dynamics. As the internuclear distance increases, there is a sharp decrease in KER over the first 150 fs (Fig. 3B). The internuclear distances corresponding to the transition region between 50 and 150 fs range from ~ 2 to 6 \AA . (From Eq. 2 we can relate time and distance, and both are labeled in Fig. 3A.) This transition represents a rapid change from an almost spherically symmetric initial binding potential for the outer excited electron to a final two-center potential at larger internuclear distances. In terms of the internuclear potential, the molecule transitions from an almost purely repulsive interaction between two charged N⁺ cores (where the excited electron does not play a strong role) to a regime in which the excited electron screens the Coulomb repulsion between the two N⁺ cores. This transition can be seen as a change in the wave function for the antibonding 4su orbital (Fig. 3A). At $r = 1.1 \text{ \AA}$, there is almost no electron density between the two nuclei (orange in Fig. 3A). However, at separations $> 3 \text{ \AA}$, the electron density between two nuclei is substantial, and the two-center nature of the potential is apparent. Past this transition region, the excited-state potential-energy curve is essentially flat, which reflects the loss of the long-range $1/r$ Coulomb repulsion between two cores as one of the partners becomes uncharged. For times > 150 fs, the KER data exhibit a complex structure suggestive of two-center quantum interferences. These rapid electronic dynamics will be an interesting topic for further study.

In the future, this work can be extended to a range of atomic and molecular systems to explore complex, correlated electron dynamics and highly excited states. Interesting topics such as the

attosecond dynamics of electron transitions, the observation of ultrafast electron transfer in molecules, and the influence of molecular structure on these x-ray driven dynamics are challenging problems that are now accessible with the use of the techniques illustrated here.

References

1. A. H. Zewail, *Science* **242**, 1645 (1988).
2. O. Geßner *et al.*, *Science* **311**, 219 (2006).
3. A. M. Rijs, M. H. M. Janssen, E. T. H. Chrysostom, C. C. Hayden, *Phys. Rev. Lett.* **92**, 123002 (2004).
4. M. H. Kim, L. Shen, H. Tao, T. J. Martinez, A. G. Suits, *Science* **315**, 1561 (2007).
5. A. Stolow, A. E. Bragg, D. M. Neumark, *Chem. Rev.* **104**, 1719 (2004).
6. S. Zamith *et al.*, *J. Chem. Phys.* **119**, 3763 (2003).
7. R. R. Meier, *Space Sci. Rev.* **58**, 1 (1991).
8. H. Imanaka, M. A. Smith, *Geophys. Res. Lett.* **34**, L02204 (2007).
9. U. Becker, D. A. Shirley, Eds., *VUV and Soft X-Ray Photoionisation* (Plenum, New York, 1996).
10. H. C. Kapteyn, M. M. Murnane, I. P. Christov, *Phys. Today* **58**, 39 (2005).
11. Y. Hatano, *Phys. Rep.* **313**, 109 (1999).
12. A. Scrinzi, M. Y. Ivanov, R. Kienberger, D. M. Villeneuve, *J. Phys. B At. Mol. Opt. Phys.* **39**, R1 (2006).
13. M. Uiberacker *et al.*, *Nature* **446**, 627 (2007).
14. L. Nugent-Glandorf *et al.*, *Phys. Rev. Lett.* **87**, 193002 (2001).
15. N. L. Wagner *et al.*, *Proc. Natl. Acad. Sci. U.S.A.* **103**, 13279 (2006).

16. L. Miaja-Avila *et al.*, *Phys. Rev. Lett.* **97**, 113604 (2006).
17. J. Ullrich *et al.*, *Rep. Prog. Phys.* **66**, 1463 (2003).
18. A. S. Alnaser *et al.*, *Phys. Rev. Lett.* **93**, 113003 (2004).
19. T. Weber *et al.*, *Nature* **431**, 437 (2004).
20. H. D. Cohen, U. Fano, *Phys. Rev.* **150**, 30 (1966).
21. A. Rundquist *et al.*, *Science* **280**, 1412 (1998).
22. S. Krummacher, V. Schmidt, F. Wuilleumier, *J. Phys. B At. Mol. Opt. Phys.* **13**, 3993 (1980).
23. Using 43.2-eV photons from a synchrotron, the partial cross section for inner-valence ionized states between 23 and 43 eV was measured to be 33% of the total photoionization cross section (22).
24. T. Aoto *et al.*, *J. Chem. Phys.* **124**, 234306 (2006).
25. J. H. D. Eland, E. J. Duerr, *Chem. Phys.* **229**, 13 (1998).
26. P. Baltzer, M. Larsson, K. Karlsson, B. Wannberg, M. C. Gothe, *Phys. Rev. A* **46**, 5545 (1992).
27. Some examples of such dissociation limits are $(N, N^+) = (^3P, ^2P_0)$, $(^1S, ^4S_0)$, $(^1D, ^2D_0)$, and $(^1D, ^2P_0)$.
28. This strong feature is probably due to the concentration of the $^2\Sigma_g^+$ oscillator strength in the region ranging from 27 to 31 eV (F-band). Dissociation from this band gives rise to a quasi-monoenergetic photoelectron peak, with a corresponding well-defined KER. The observed electronenergy width results from the soft x-ray pulse bandwidth.
29. We identify and distinguish bound and dissociative channels in the supporting online material. The triple coincidence data presented in fig. S1 confirms that we selectively probed highly excited dissociative states near the double-ionization threshold of N_2 .

30. M. Lundqvist, D. Edvardsson, P. Baltzer, B. Wannberg, *J. Phys. B At. Mol. Opt. Phys.* **29**, 1489 (1996).
31. H. Sambe, D. E. Ramaker, *Chem. Phys.* **107**, 351 (1986).
32. D. Dill, J. L. Dehmer, *J. Chem. Phys.* **61**, 692 (1974).
33. We thank A. Czasch, T. Jahnke, A. Paul, W. Li, and B. Walker for technical support and useful discussions. We acknowledge support for this work from the NSF through the Physics Frontiers Centers Program and from the Department of Energy, Office of Science. This work made use of facilities provided by the NSF Engineering Research Center on Extreme Ultraviolet Science and Technology

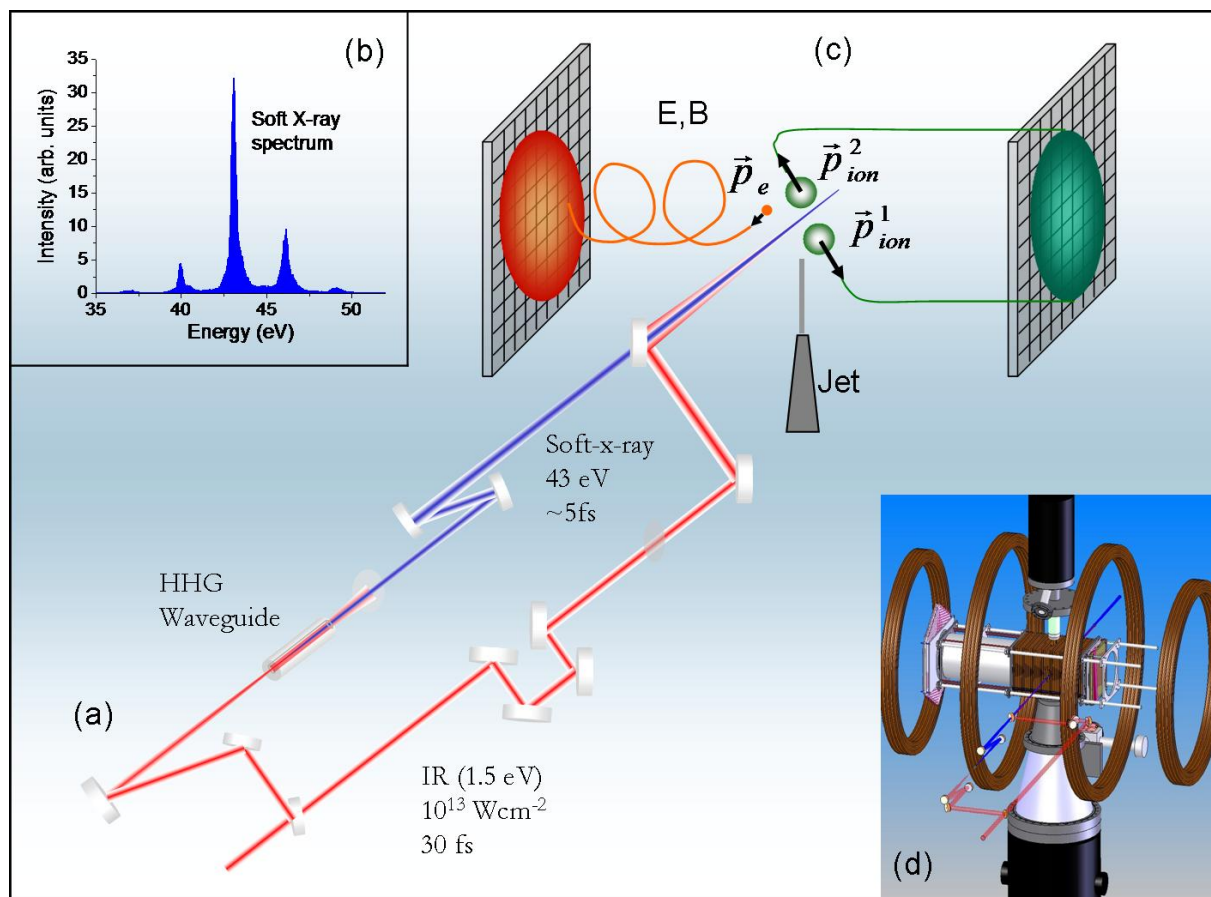


Figure 1. (a) Experimental setup to probe radiation-induced dynamics. High harmonic pulses centered at 43eV are generated in a waveguide to serve as the pump beam. An IR laser beam serves as the probe. (b) Spectrum of the soft-x-ray pulse after reflection from two multilayer mirrors. (c) Inside the reaction microscope. After the soft-x-rays interact with a supersonic N_2 gas jet, uniform electric and magnetic fields guide the reaction fragments to position-sensitive detectors. The combined position and time-of-flight information yields the vector momentum of each fragment in coincidence. (d) Exterior schematic of the reaction microscope.

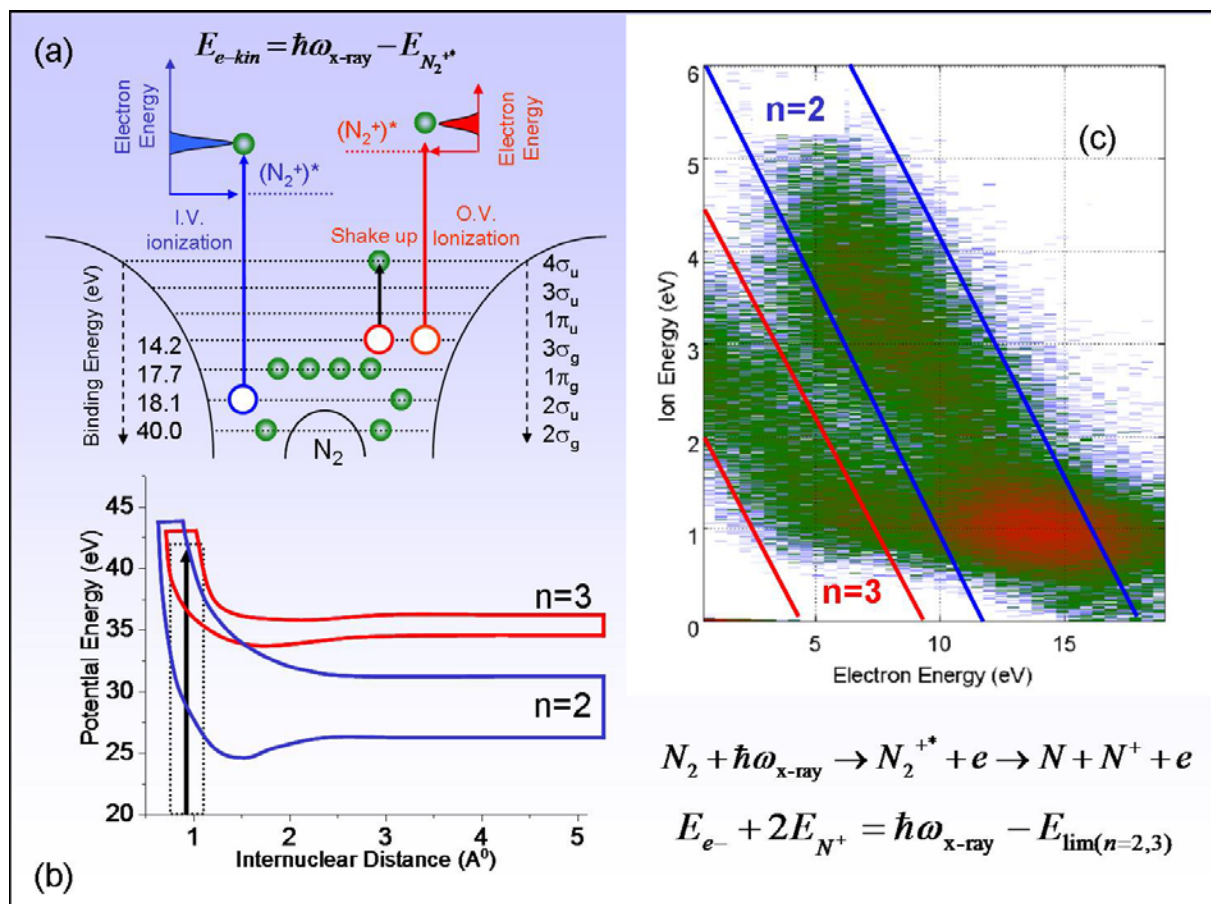


Figure 2. (a) Schematic of the formation of highly excited N_2^+ through an inner-valence (i.v.) ionization process (blue), or an electron shakeup process (red) accompanying outer-valence (o.v.) ionization. The electron binding energies are listed on the left while the orbitals are labeled on the right. (b) Schematic of the predominant dissociation channels of N_2^{+*} , where the inner-valence ionization channel is labeled in blue and the shakeup channel is labeled in red. The 43 eV soft-x-ray photon (black arrow), Franck Condon excitation region (dotted lines) and the dissociation limits (atomic states: $n=2,3$) are indicated. (c) Recoil and electron energy correlation diagram for the dissociation of N_2 initiated by an ultrafast soft-x-ray pulse.

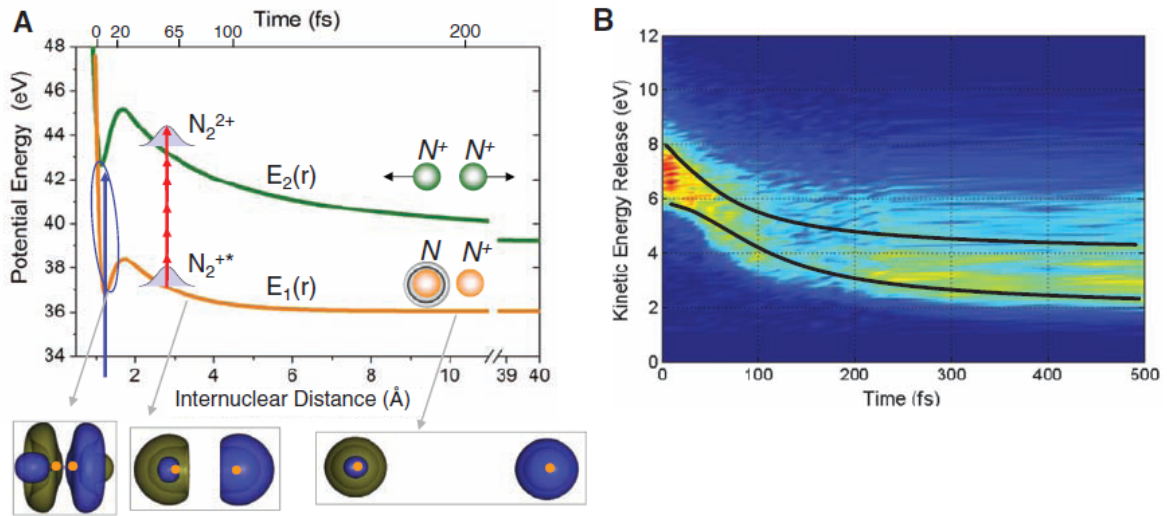


Fig. 3. (A) A soft x-ray pump pulse photoionizes N₂ to a highly excited N₂^{+*} shakeup state [orange curve labeled E₁(r)]. The probe IR pulse further ionizes N₂^{+*} to the final N₂²⁺ ground state, shown in green and labeled E₂(r). The N₂²⁺ potential curve was adapted from (30), whereas the N₂^{+*} curve was calculated as described in the text. A schematic of the wave function for the N₂^{+*} state is also shown at different internuclear separations. **(B)** Evolution of the ion KER in the N⁺/N⁺ channel as a function of time delay between the 5-fs soft x-ray pump pulse and the IR probe pulse. The experimental data were not normalized for the long-term drift in EUV flux levels of 15% over a 2-day time period. The theoretically calculated KER for the 4su electron shakeup is plotted as a band. The lower limit for this band is imposed by the local potential minimum of the N₂^{+*} and also by the potential barrier of the N₂²⁺ state for time delays near zero. The upper limit is set by the width of the N₂ ground-state wave packet, i.e., the width of the Frank Condon region [blue region of the E₁(r) curve in (A)].

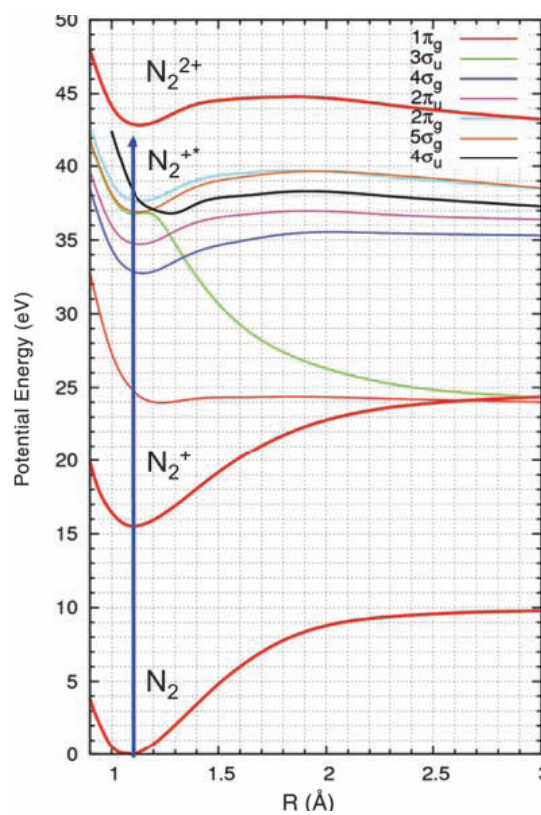


Fig. 4. Calculated N_2^{+*} states resulting from an electron-shakeup process. These states consist of a loosely bound electron surrounding a doubly charged N_2^{2+} core. The black curve corresponding to the $4s_u$ electron shakeup is predominantly populated because of the large overlap with the valence orbital. This shakeup state corresponds to the excited state $E_1(r)$ (shown in Fig. 3A). It was also used to calculate the theoretical KER band (shown in black in Fig. 3B).

Supporting Online Material:

Supporting Text: Identifying and separating bound and dissociative channels

The N_2^{2+} ion exhibits a potential well in the Franck-Condon region, and thus has a metastable component (*S1*). Near zero pump-probe time delays, we observe the formation of N_2^{2+} ions (Fig. S1A), which can be directly observed by their zero ion recoil energy. This process is akin to a direct multiphoton double ionization involving a single soft-x-ray photon and several IR photons. With increasing time delays, the N_2^{2+} ion yield decreases to a baseline value, which is the same as the yield due to x-ray excitation alone. A Gaussian fit to the N_2^{2+} ion yield as a function of pump-probe delay gives a width of 30 fs (Fig. S1A), that is comparable to the IR pulse duration (28 fs) and longer than the softx-ray pulse duration (~5fs). These data therefore imply that most of the metastable N_2^{2+} ions are generated instantly, when both the soft-x-ray and IR fields are present simultaneously. Because the N_2^{2+} ion production ceases when the IR probe pulse is delayed by ~20 fs relative to the soft-x-ray pump pulse, we can infer that after this time, the N_2^{2+} is already too far advanced in the process of dissociating to N^+/N for multiphoton ionization to form bound N_2^{2+} states.

Multiphoton ionization at later times leads to kinetic energy release sufficient to overcome the local N_2^{2+} potential minimum, leading to further dissociation on the N_2^{2+} ground state potential curve. This dissociation (Coulomb explosion) results in the formation of two N^+ fragments with equal and opposite momenta. The ion kinetic energy release for this N^+/N^+ explosion channel, requiring two ions and one electron in coincidence, is plotted versus electron energy in Fig. S1B, for a pump-probe time delay of ~30 fs. We observe electron energies less than 4 eV and ion kinetic energy releases between 6 and 8 eV. The observed electrons could be a result of either x-ray photoionization or IR probe induced multiphoton ionization. Low electron kinetic energy

implies that we are probing the dynamics of high excited states which lie very close to the double ionization threshold. The limits of kinetic energy release (6 to 8 eV) are determined by the vibrational spread of the excited ionic states and the potential barrier of the final N_2^{2+} state. In the absence of the IR field, we do not observe any counts in the correlated N^+/N^+ channel. Thus, by detecting the correlated N^+/N^+ channel arising from the collective action of the soft-x-ray pump and IR probe, we can cleanly probe the evolution of an N_2^{+*} dissociating wave packet, free of background contamination from other N^+ ions.

References

S1. M. Lundqvist *et al.*, *J. Phys. B* **29**, 1489 (1996).

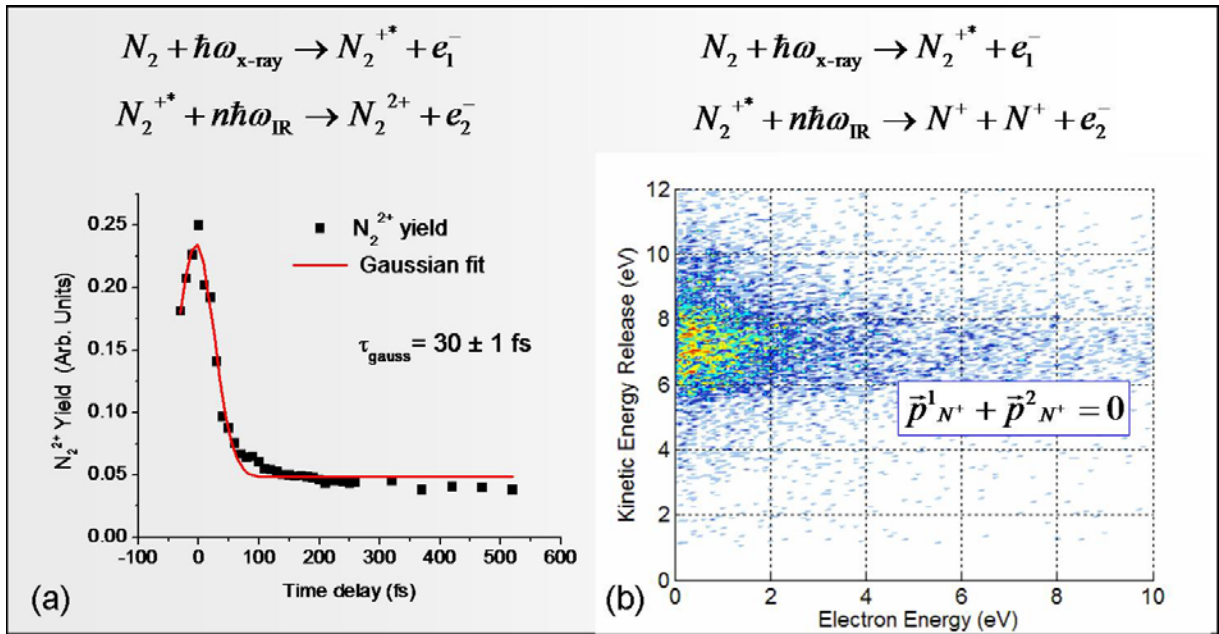


Figure S1. (A) Metastable N_2^{2+} yield as a function of time delay between the soft-x-ray pump and the IR probe. (B) Ion kinetic energy release vs coincident electron energy for the dissociative final state that leads to the formation of two N^+ ions with equal and opposite momentum, at a time delay of 30 fs between the soft-x-ray and IR pulses.